Journal Pre-proofs

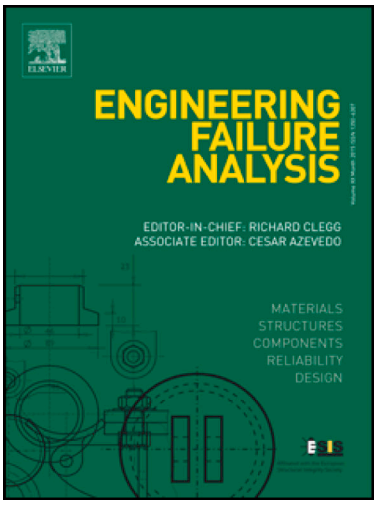

Crack Growth models for multiaxial fatigue in a ship's propeller shaft

Vidar Hellum, Tom Lassen, Andrea Spagnoli

PII: S1350-6307(21)00330-7
DOI: https://doi.org/10.1016/j.engfailanal.2021.105470
Reference: EFA 105470

To appear in: *Engineering Failure Analysis*

Received Date: 12 February 2021
Revised Date: 30 April 2021
Accepted Date: 9 May 2021

Please cite this article as: Hellum, V., Lassen, T., Spagnoli, A., Crack Growth models for multiaxial fatigue in a ship's propeller shaft, *Engineering Failure Analysis* (2021), doi: https://doi.org/10.1016/j.engfailanal.2021.105470

Crack Growth models for multiaxial fatigue in a ship's propeller shaft

By Vidar Hellum[1], Tom Lassen[1] and Andrea Spagnoli[2]

[1]University of Agder, Grimstad, Norway

[2]University of Parma, Parma, Italy

Abstract

A premature fatigue failure of a large intermediate propeller shaft in a shuttle tanker is discussed and analyzed. The short fatigue life consists mainly of a crack growth phase. Life predictions are carried out by crack growth modelling based on engineering fracture mechanics. The purpose of the present investigation is to identify the most likely loading modes based on the evolution of the crack propagation. A Linear Elastic Fracture Mechanics Model (LEFM) is applied with the stress intensity factor range entering the Paris law as a key parameter. Existing formulas for the geometry functions are supplemented by more detailed stress intensity factor calculations pertaining to small semi-elliptical surface cracks subjected to stress mode I. Enhanced geometry functions are proposed as a function of the relative crack depth and the crack shape aspect ratio. The ability of the fracture mechanics model to reconstruct the observed crack path and crack shape development is emphasized. Various loading modes and multi-axial stress states are applied to pursue the observed crack behavior. The observed semi-elliptical crack shapes and the shift in crack planes are included in the analysis.

Keywords:

Propeller shaft

Stress intensity factors

Fatigue crack propagation

Multi-axial stress states

1 Introduction

Shuttle tankers are widely used for oil transport from the installations in the North Sea to oil refinement plants onshore. Lack of reliability against power failures is of major concern to avoid incidents such as collision with platforms. The most common machinery related damages experienced are those to propeller shafts and engine bearings[1]. On this background the fatigue failure of the intermediate steel propeller shaft onboard a shuttle tanker is analyzed. The fracture occurred after 20 months of service time only. The fracture appeared on the uniform cylindrical part of the shaft and not in the vicinity of any geometrical stress concentration. The short fatigue life was caused by a surface defect that acted as a starting point for crack propagation. A sketch of the engine and shaft lay-out is shown in Figure 1. The shaft has a diameter of 360 mm and is made of high strength carbon steel with a yield stress of 540 MPa. The location of the fracture is also indicated.

When such in-service failures occur, the failure investigation is often characterized by two challenges. The first challenge is the lack of information; the second challenge is the need for correct decision to prevent failures of similar shafts still in service. To tackle the situation, a thorough examination of the design criteria, service conditions and damage appearance must be carried out. Then, failure hypotheses must be proposed and rejected based on available evidence. In the present case it was obviously a fatigue failure, and the damage mechanism was primarily crack growth. The dominant loading mode and stress levels are not exactly known. Linear Elastic Fracture Mechanics (LEFM) was used in conjunction with Paris law to determine the evolution of the crack under various assumptions. To carry out the necessary calculations of the Stress Intensity Factor (SIF), the size of the initial crack and the crack shape evolution during propagation must be known. Based on the given fatigue life and on inspection of the fatigue fracture surface, a detailed study was carried out to determine the crack growth path and corresponding most likely loading mode.

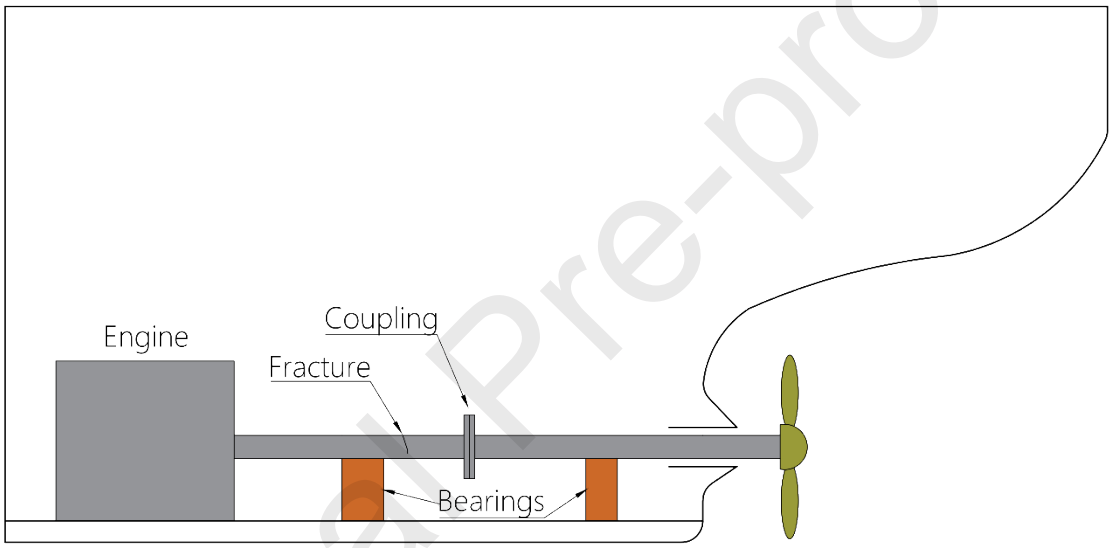

Figure 1 Sketch of shaft lay-out and location of fracture

The scope of the present work is both theoretical and practical. It is demonstrated how detailed fracture mechanics modelling can reveal the dominant loading modes and stress levels. One of the main objectives for the work is to demonstrate that the recent advancements in engineering fracture mechanics provide a model that can simulate the evolution of the fatigue damage with crack propagation as the dominating phase. Various loading modes and observed shift in crack planes during the crack evolution are included in the analysis. Practical preventive measures to avoid similar failures are shortly discussed and some recommendations are given.

2 Design criteria, load conditions and steel properties

2.1 Design requirements and class notation

The classification societies give rules and regulations for the shaft design. An example is given by the current version of DNVGL rules for ships[2] that includes a section for design and requirements for shafts which should be followed if the vessel is subject to DNVGL class approval. Two methods for finding the required diameter for the shaft is provided; a simplified method based on the power rating of the system along with the shaft speed and the specified minimum tensile strength of the

shaft material, and a more detailed method given in DNVGL-CG-0038 Calculation of shafts in marine applications[3]. The simplified method is considered the more conservative of the two and will provide larger diameters. The simplified method should provide sufficient safety against fatigue failure and local deformation when the load conditions presented in section 3 is accounted for. Both methods are based on an S-N methodology for fatigue life assessment.

2.2 Steel properties

The shaft steel is a 42CrMo4 forged steel delivered in quenched and tempered condition. Corrosion resistance is obtained by coating. The mechanical properties and the chemical composition of the shaft steel are retrieved from material certificates where it is found that the tensile properties have been retrieved by testing of Ø10mm round specimens. The mechanical properties and the chemical composition are given in Table 1 and Table 2. It is a plain shaft with a surface roughness of 20 microns, peak to valley.

Table 1 Mechanical properties

Tensile properties				Charpy V-notch impact properties			
Yield point [MPa]	Tensile strength [MPa]	Elongation [%]	Reduction of area [%]	Orientation	Test temp [°C]	Width of test piece [mm]	Energy [J, min]
Min 540	Min 800	12	34	T	+20	10 x 10	41

Table 2 Chemical composition

Element	C	Mn	Si	P	S	Cr	Ni	Mo	Cu
Specific values	0.38 to 0.45	0.6 to 0.9	Max 0.40	Max 0.035	Max 0.035	0.9 to 1.2	Max o.40	0.15 to 0.30	Max 0.30

2.3 Design criteria, shaft speed and rated power

The shaft covered in the present work was considered to be mainly subject to torsion and the simplified method for determining the minimum diameter of the shaft when there is no shaft bore is given as[2]:

$$d_{min} = 100 \cdot \sqrt[3]{\frac{P}{n_0} \cdot \frac{560}{\sigma_B + 160}} \quad (1)$$

Where n_0 is the shaft speed in rpm at rated power, P is the rated power transmitted through the shaft and σ_B is the specified minimum tensile strength in MPa of the shaft material. The rated power for the engine is 10010kW and the nominal speed is 127 rpm. Using this simplified criterion, the minimum diameter required for the shaft is 358mm. The chosen diameter is 360 mm.

3 More detailed assessment of the load conditions

A schematic time history of possible stresses in a given cross-section of the shaft is shown in Figure 2. The graphs are from a start situation to the completion of a given voyage.

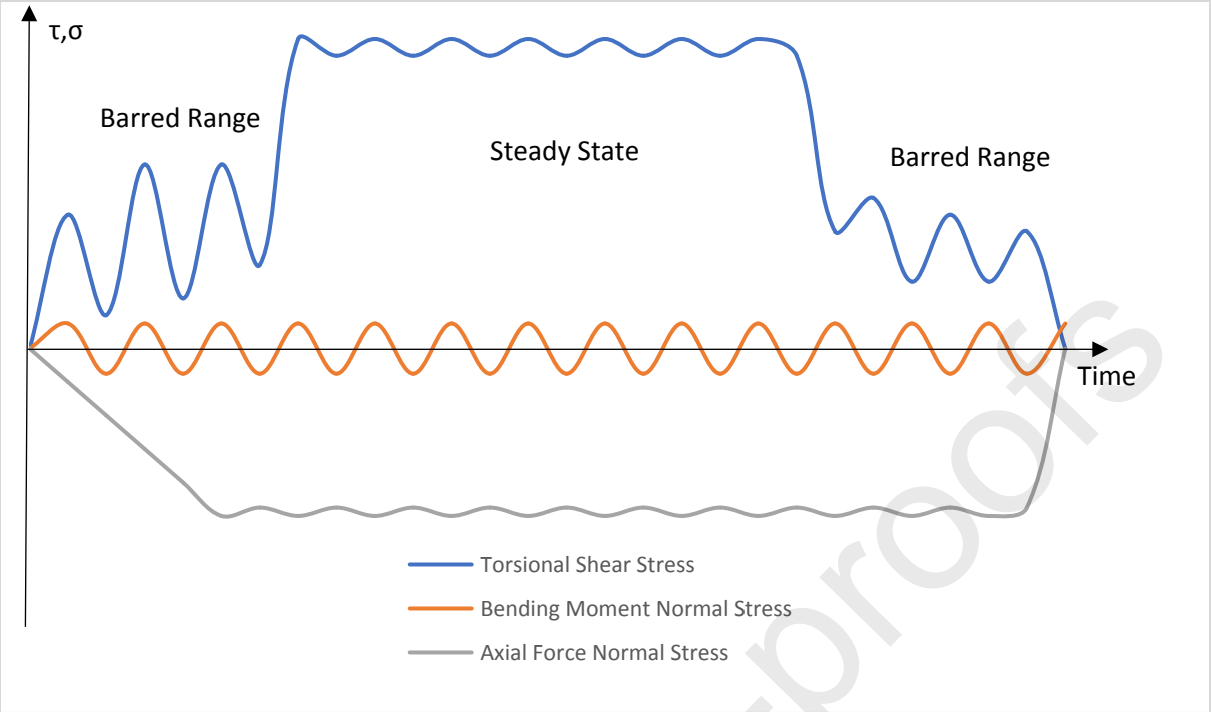

Figure 2 Schematic time history of possible stresses in shaft cross-section during a single voyage

As can be seen in Figure 2 the main stress components are the torsional shear stresses and the normal stresses due to the thrust force. These curves give a large global variation for both stress histories, but only as one defined load cycle. Reversing loads are not considered in the present case. Shuttle tankers usually have more cycles of these large stress amplitudes than commercial tankers due to relatively short durations of the many missions. Both stress types may have dynamic intermediate variations characterized by smaller amplitudes but with large number of cycles. Normal stresses induced by the thrust force are mainly compressive and are commonly not regarded as critical to the fatigue life of the shafts. Hence, these stresses are neglected in the present analysis. The shear stresses have large variation at a critical frequency occurring at the beginning and at the end at a relatively low frequency. However, this situation lasts only for a short while due to definition of a barred speed range for the actual critical torsional frequency. Due to the importance of this shear stress resonance phenomenon, testing is carried out and the main result is given by the graph shown in Figure 3. The critical speed and the steady state shear stress amplitudes are determined.

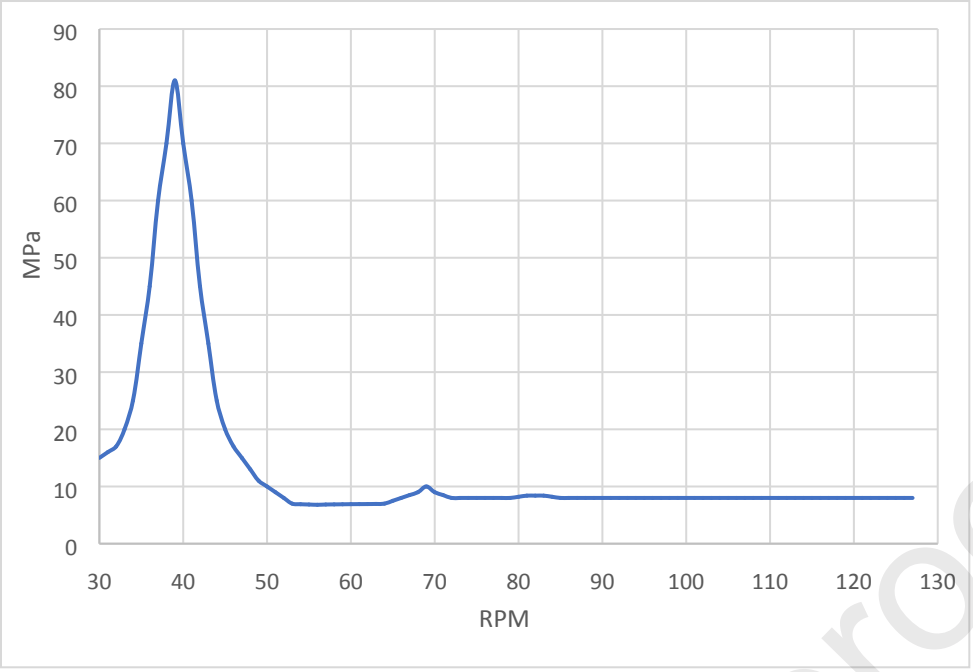

Figure 3 Measured torsional vibrations

In addition to the foreseen stress variations discussed above, one may have normal stresses due to unintentional bending of the shaft. These bending stresses are introduced due to lateral loading from the propeller and/or by lack of alignment of the shaft bearings. The stress variations are dependent on the number and order of the propeller blades. In addition, the dynamic bending effect may increase due to bearing misalignment. The shaft alignment is usually performed in a static loading condition for the hull beam. When in service, the boundary conditions of the shaft may be different than for the chosen static condition due to the flexible hull behavior. In addition, the contact points on the bearings are difficult to model correctly which might contribute to misalignment [1], [4]. If the frequency is close to one of the eigen frequencies of the shaft the bending stress variations will become more severe. A further discussion of these topics is given in [5].

Based on the above discussion the critical loading modes with corresponding stresses are shown in Figure 4. The fatigue stress spectrum can be summarized as follows:

- Low cycle fatigue stress variation due to variations from 0 to full load, clutching-in chock loads, reversing torques, etc. For a shuttle tanker which might be considered as a special case the number of cycles for this condition could be up to 10^5
- High cycle fatigue stress variation due to rotating bending and torsional vibration where more than $3*10^6$ cycles should be considered
- Transient vibration when passing through a barred speed range where the number of cycles should be in the range 10^4 to $3*10^6$

Figure 4 Critical Loading modes for fatigue in propeller shafts and associated stresses

This stress spectrum gives a combination of normal stresses and shear stresses introduced by bending and torsion which may contribute to fatigue damage accumulation. The two stress components may act in a proportional or non-proportional manner depending on the phase correlation between the loads and associated stresses. Many rules and regulations as for example DNVGL-RP-C203 incorporates multiaxial loading by using the maximum principal stress as the driving force for crack propagation and fatigue damage calculations. This implies mode I crack growth.

For in-phase loading, the direction of the principal stress axis will be constant, whereas for out of phase loading the direction of the principal axis will vary. It is argued by several authors that the fatigue damage might be accelerated when a component is subject to out-of-phase multiaxial fatigue loading due to additional cyclic hardening [6][7]. This is important knowledge but will not be pursued during further discussions in the present paper. However, multiaxial loading and crack plane orientation will be discussed in section 6.2.

4 Important observations and description of the fracture

The fracture occurred in the intermediate shaft as shown in Figure 1. The shaft is uniform on the given location without any notches and associated stress concentrations. The fractured surface is shown in Figure 5. As can be seen, the crack has obviously started from one single point at the shaft surface. There are semi-elliptical shaped beach marks on the surface that gives the position of the crack front at various stages during the crack propagation. The fracture surface is characterized by its smooth appearance with almost no plastic strain in the beginning. These are typical observations leading to the conclusion that the fracture is a failure caused by a fatigue damage mechanism. The beach marks are introduced when the shaft is running at low speed with low variations in the acting fatigue stresses. Microscopy analysis of the crack initiation location indicated a heat related irregular shaped surface defect with several micro planes. It could not be categorized as a crack-like flaw but is modelled as such during crack propagation analyses. The depth of the defect was between 0.5 mm and 1.0 mm. Pursuing the source of this defect was not conclusive, but one hypothesis is that it was caused by a weld arc strike. At an early stage up to a crack depth of 9 mm the crack planes are almost perpendicular to the shaft axis. At larger crack depths the crack plane shifts towards a 60 degrees inclination with respect to the shaft axis as shown in Figure 6. The final rupture is ductile and occurs at a crack depth close to 250 mm. At this stage, the remaining ligament of the shaft is overloaded, and large-scale yielding is occurring. The expected 45 degrees shear planes for this damage mechanism can clearly be seen in the bottom of Figure 5.

To characterize the evolution of the crack geometry, five chosen crack fronts were studied in detail, see Figure 7. The crack aspect ratio a/c is an important variable for identifying the dominant loading mode during the propagation. Each crack front in Figure 7 is designated by a number and for crack no 2-5 the associated label has its down left corner located where the actual crack front intersects with the free surface of the shaft. The shape data of the cracks according to the notation of Figure 8 are given in Table 3. The table also shows the shift in crack plane angle during crack propagation. The smallest crack designated no 1 is difficult to trace and the geometry is somewhat uncertain. It has a smaller aspect ratio than the others and is most likely formed by the coalescence of several circular shaped small cracks. All the other cracks are semi-elliptical with a rather high aspect ratio a/c. The fatigue crack plane is normal to the shaft axis for crack front no 1 and when approaching crack front no 2. After the crack depth passes 9.2 mm (crack no 2, a/d=0.026, a/c=0.75) the fatigue crack plane shifts towards an angle of 60° with respect to the shaft axis as shown on the drawing in Figure 6.

Table 3 Crack shape data

Crack no	Crack depth a[mm]	a/d	a/c	Crack plane angle relative shaft axis
1	5.4	0.015	-	90
2	9.2	0.026	0.75	60
3	25.2	0.07	0.89	60
4	36	0.10	0.76	60
5	90	0.25	0.82	60
Final fracture	250	-	-	+-45

Figure 5 Fractured propeller shaft

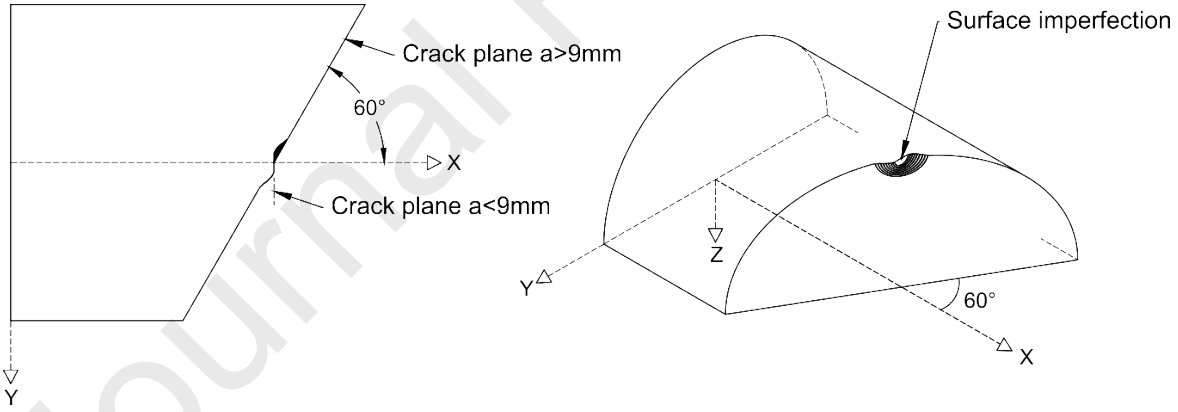

Figure 6 Crack plane development relative to shaft axis. Left segment seen from top of figure 5, right segment is an isometric view towards the crack plane

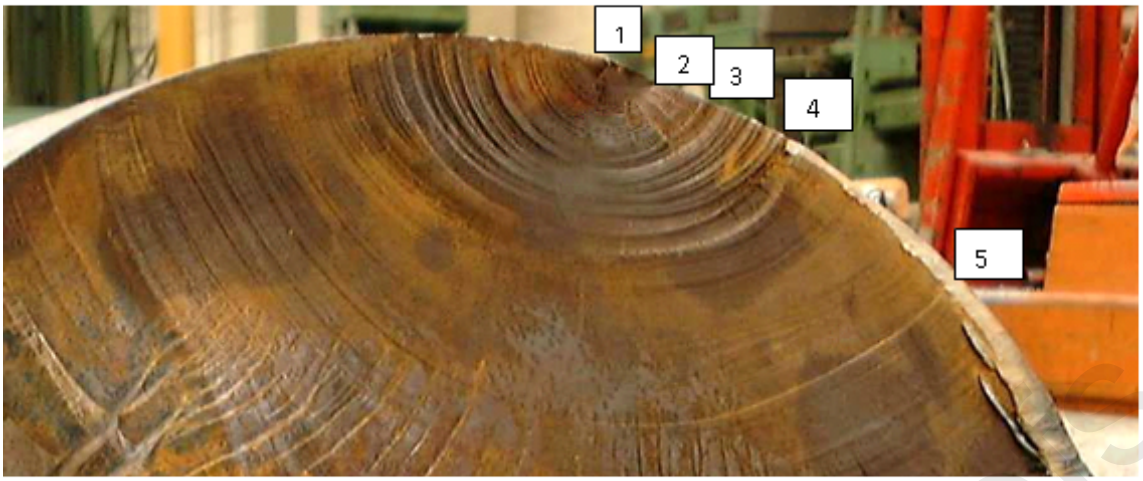

Figure 7 Crack shapes

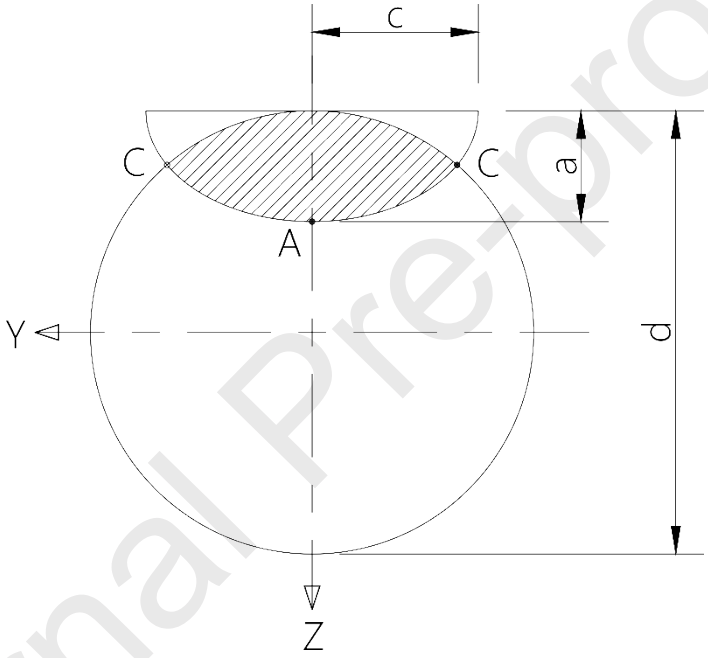

Figure 8 Crack shape definition

5 Basis for crack growth investigations

5.1 General considerations

The conclusion from section 4 is that the fracture has been driven by fatigue damage mechanisms dominated by crack growth. However, we have not yet gone into the various stages and possible details involved in the damage evolution. The fatigue damage process before final fracture is often explained by the following three phases[8], [9]:

- Phase 1: Crack nucleation. The cracks initiate due to repeated irreversible plastic deformation at irregularities in the microstructure, e.g. at dislocations and grain boundaries. The cracks may initiate close to the surface or at the surface
- Phase 2: Growth of micro cracks with crack sizes down to the grain size of the microstructure typically in the range from 10 to 100 µm. The damage process may involve crack coalescence between multiple cracks and crack arrest.
- Phase 3: Growth of larger cracks with depths beyond 100 µm

It is generally accepted that phase 1 and phase 2 are important parts of the fatigue damage evolution in high quality machined parts with a smooth surface. Detailed discussions on the subject can be found in publications by Miller[10], [11].

Based on the discussion of the crack shape evolution given in section 4 it can be concluded that the crack nucleation phase and the micro crack growth described above hardly have been present for the present propeller shaft. This is very surprising because these two phases usually represent the dominant part of the fatigue life in a high strength forged shaft steel. The presence of a defect on the shaft surface has dramatically weakened the fatigue strength and shortened the fatigue life. The experienced short fatigue life is dominated by a large crack growth phase as described above. This phase will be further investigated to identify the most likely loading modes and the stress spectra. The crack evolution given in Table 3 will be simulated by applying engineering fracture mechanics crack growth laws. The objective is to validate that these theoretical models have matured into a stage where they can simulate a practical in-service realistic crack evolution. The multi-axial stress state and the associated shift in fatigue crack planes are at the essence of the investigation.

6 Crack growth modelling

6.1 Definition of crack geometry

Various crack shape definitions for cracks in round bars can be found in the literature including [12]–[16]. In the present work the crack shape definition presented in Figure 8 that is based on the definition given by Carpinteri [12], [16] will be used. The crack front is described by a semi-elliptical shape given by equation 2, with depth a, and crack aspect ratio a/c, where c is half the major axis of the ellipse.

$$\frac{y^2}{c^2} + \frac{z^2}{a^2} = 1 \qquad (2)$$

The surface points of the crack are denoted C and the deepest point of the crack denoted A. The two outer limits of the shape definition are when a/c=1, which is a semi-circular shape and when a/c=0, which is a straight fronted crack.

6.2 Loading modes and stress situation at the crack

In fracture mechanics theory there are three different ways of defining the stress situation based on how the stresses are acting at the crack front. If the stresses act normal to the crack plane and moves the crack planes directly apart the stress situation is denoted crack tip stress mode I. When the crack

planes are subject to shear stresses normal or parallel to the crack front, the stress situation is denoted crack tip stress mode II and III respectively. If more than one stress mode is present on the crack plane, the crack is subject to a mixed crack tip stress mode. The two main challenges with mixed stress mode propagation are to determine the crack growth plane and the crack growth rate.

Several authors[17]–[20] argue that cracks subject to mixed stress mode propagation or even mode II or III separately will quickly develop into a path governed by stress mode I. Hence, a crack emanating from an initial crack-like flaw which is oriented in such a manner that the crack plane is only subject to shear stresses, will experience a crack development where the crack plane rotates during further growth into a crack plane normal to the maximum principal stress direction. The subsequent growth will thus be governed by stress Mode I.

However, the paths of cracks subject to mixed mode loading are complex and still a research field subject to differing theories. Qian and Fatemi performed a literature study on the subject, and the lack of standardized test specimens for mixed mode fatigue crack growth experiments were emphasized[21]. Pook[18] performed testing on a three point bending specimen with an inclined crack leading to a combination of stress mode I and III. His tests showed that the crack gradually rotated towards a perpendicular plane relative to a pure stress mode I, driven by maximum principal stresses. Yates et. al.[20] also supported this gradual change towards stress mode I for cracks initially subject to stress mode I and mode III but argued that the initial crack path can be complex and chaotic. The definition of crack plane orientation which will be referred to in the present paper is shown in Figure 9 where the angle Θ is measured from the shaft axis. The figure shows a crack plane which has started as perpendicular to the shaft axis and rotated to a crack plane with angle Θ at a later stage. This is similar to the observed behavior in the present case.

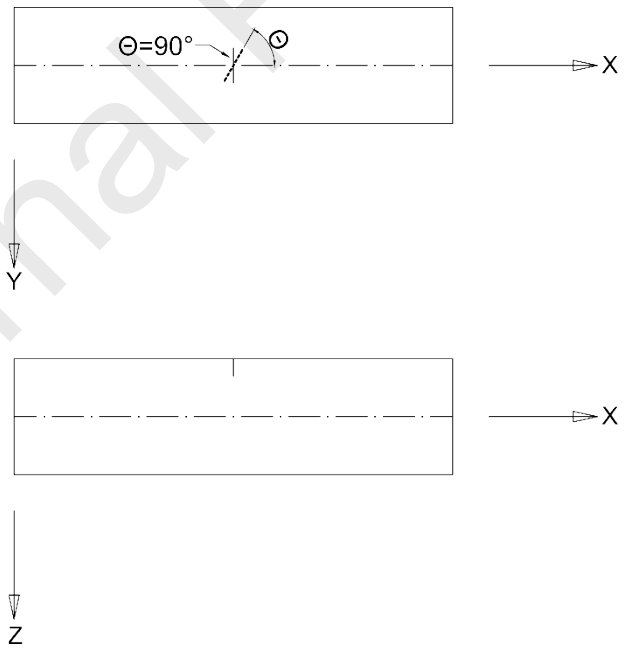

Figure 9 Definition of crack plane orientation for a shaft

Different criteria are proposed for predicting the crack path when using the stress components σ_x and τ_{xy} acting on an initial crack plane Θ=90 degrees.

If applying Sih's strain energy density criterion[22] as explained by Richard et al[23], the predicted crack path will always remain in the Θ=90 degrees plane. Hence, a mixed mode calculation involving stress mode I, II and III must be performed on this plane to investigate the growth rate.

Pook on the other hand proposed that the crack path could be determined based on the stress intensity factors for the different stress modes.

Pook's criterion will predict an angle between $45° \leq \Theta \leq 90°$ where Θ is the angle between the crack plane and the shaft length axis, see Figure 9.

Where Θ=90 degrees when only subject to stress mode I

And Θ=45 degrees when only subject to stress mode III

Richard et al[24] proposed a method for calculating the crack path which is very similar to the method proposed by Pook. Following this method, the crack path can be calculated according to equation 3:

$$\Theta = 90° - \left[C\frac{|K_{III}|}{K_I + |K_{II}| + |K_{III}|} + D\left(\frac{|K_{III}|}{K_I + |K_{II}| + |K_{III}|}\right)^2 \right] \quad (3)$$

Where Richard et. al. propose to use the values C=78 degrees and D=-33 degrees which they argue give good agreement with crack planes they observed.

Both the criterion of Pook and the criterion of Richard et al implies that the crack plane rotates towards a crack plane orientation where only stress mode I will be present. Hence, establishing the crack path using this equation should not be combined with a crack growth analysis based on mixed crack tip stress mode.

Based on the references and the above discussion it may be concluded that for the various possible loading modes in a shaft, there are three cases with different orientation of the fatigue crack planes:

1. If the bending loading mode is dominant, the crack planes will be normal to the shaft axis. The crack will grow under a stress mode I mechanism.
2. If the torsional loading mode is dominant which is expected for a propeller shaft, the crack plane will form a 45 degrees helix shaped plane as reported in [25]. At this plane the crack will grow under a stress mode I mechanism as in case 1
3. If the shaft is subjected to a combination of torsion and bending loading modes, there will be two options for the crack planes:
   a) Although the acting normal and shear stresses are of the same magnitude it is still the normal stress that governs the orientation of the crack planes. The plane orientation will remain 90 degrees to the shaft axis as in case 1 above. The crack will primarily grow under stress mode I but mode II and III may accelerate the crack growth by an interaction between the stress modes at the given perpendicular plane. There will be a mixed stress mode crack growth at the crack front
   b) The crack plane will be a function of the three stress modes at the crack front and the crack plane may shift to the plane perpendicular to the largest principal stress. The crack plane will seek an orientation between the case 1 and 2 above, i.e. the plane will have an angle between 45 and 90 degrees to the shaft axis. At this plane the crack will grow under a stress mode I mechanism as in case 1

The first two cases are the most common ones for dynamically loaded shafts. These cases are well known to and handled by the mechanical engineering community. The first propagation mechanism is avoided by a proper alignment of the shaft such that crack initiation does not take place and the propagation phase described above is not reached during the service life. The second case is avoided by imposing barriers in the critical frequency area that generates high shear stresses. As for case 1 crack initiation will then be avoided during service life. If a crack propagation phase is reached, LEFM models for stress mode I are applicable to describe the crack growth in both cases. The basic equations and parameters entering the calculations are readily found in the engineering literature for both case 1 and 2.

The third case is a mixed mode of case 1 and 2. For this third case engineering fracture mechanics models based on LEFM for crack growth do not exists. Both sub cases are less understood, and the possible models are far less elaborated for engineering purpose. Whether case a) or b) will occur will depend on the magnitudes of the various stress components. Furthermore, the microstructure of the steel will also play a role. Structures that are more vulnerable to crack growth under stress mode I will favor case b. It is also often a common simplification that case b with stress mode I will be the one occurring for larger cracks.

6.3 Basic equations for crack growth

In the present paper, crack growth is assumed to follow Paris-Erdogan Law[26] which is based on Linear Elastic Fracture Mechanics, where the growth at the surface point C and the growth at the deepest point A is modelled by the following expressions:

$$\frac{dc}{dN} = C\Delta K_C^m \tag{4}$$

$$\frac{da}{dN} = C\Delta K_A^m \tag{5}$$

Where C and m are material constants and ΔK is the stress intensity factor range. The range of the stress intensity factor is the driving force for the crack growth in the chosen directions. It is assumed that crack growth only occurs when $\Delta K > \Delta K_{th}$, where ΔK_{th}, is a threshold value for the stress intensity factor range. The expressions for the acting SIFs for the possible stress modes are:

$$\Delta K_I = (\Delta\sigma_F \cdot Y_F + \Delta\sigma_B \cdot Y_B)\sqrt{\pi a} \tag{6}$$

$$\Delta K_{II} = \Delta\tau_T \cdot Y_{TII}\sqrt{\pi a} \tag{7}$$

$$\Delta K_{III} = \Delta\tau_T \cdot Y_{TIII}\sqrt{\pi a} \tag{8}$$

The Y factors in equation 6-8, are geometry functions dependent on the type of loading, crack shape, crack depth and the location along the crack front where the stress intensity factor calculation is performed.

Further Richard et al[24] introduced an equivalent stress intensity factor range for mixed mode loading which reads:

$$\Delta K_{eq} = \frac{\Delta K_I}{2} + \frac{1}{2}\left(\Delta K_I^2 + 4(1.155 \cdot \Delta K_{II})^2 + 4(\Delta K_{III})^2\right)^{0.5} \quad (9)$$

In this formula only proportional loading is considered. This equivalent stress intensity factor range is used in combination with Paris Law for crack growth analyses.

Crack growth can be calculated at any point along the crack front. In the present work the crack development at the two locations A and C defined in Figure 8 is chosen. Crack growth is calculated for increments of 10^6 cycles where the stress intensity factors are recalculated at the start of each increment. The propagation direction is given by a normal vector to the ellipse in the points A and C. The horizontal length L between location A and C can be found by equation 10 and furthermore equation 2 can be used for finding the z-coordinate of the initial point C based on the assumed initial aspect ratio. When the coordinates of the initial point C is known, the normal vector to the ellipse at this location can be computed and the growth direction is established.

$$L = \left(\left(\frac{d}{2}\right)^2 - z_E^2\right)^{0.5} \quad (10)$$

Where

$$z_E = \frac{\frac{d/2}{a^2} - \left(\frac{1}{a^2} - \frac{1}{c^2} + \frac{(d/2)^2}{c^4}\right)^{0.5}}{\frac{1}{a^2} - \frac{1}{c^2}} \; if \; a \neq c \quad (11)$$

To follow the crack shape development accurately, this procedure must be performed for all increments. However, when using equations 4 and 5 directly for calculating the crack development in the shaft, the deviation from the more accurate procedure described above was close to 0.01% after 1.04E+08 cycles, which indicate that this is a valid option. The calculations are carried out for the two possible plane orientations discussed at the end of section 6.2, hence both option 3a and 3b is investigated.

6.4 Calculations of the geometry factors for stress mode I

Many authors have proposed geometry factors Y for determining ΔK in round bars under stress mode I. Carpinteri investigated the geometry factor for semi-elliptical cracks at the deepest point of the crack, and close to the surface point of the crack in round bars subject to axial and bending loading as a function of the relative crack depth $\frac{a}{d}$ and the crack aspect ratio $\frac{a}{c}$ [12]. Shih and Chen performed curve fitting on the results obtained by Carpinteri to create polynomial expressions for the geometry factor[27], however the polynomial expression retrieved for bending stress does not compare well with the results presented by Carpinteri. In addition, the smallest crack included in Carpinteri's work was $\frac{a}{d} = 0.1$, which represents a relatively large crack with limited remaining fatigue life. Couroneau

and Royer presented geometry factors for cracks as small as $\frac{a}{d} = 0.05$ for loading mode I [14], whereas Lavan and Royer presented geometry factors for cracks ranging between $0 \leq \frac{a}{d} \leq 0.45$ for loading mode I, II and III[13].

For loading stress mode I, considering axially loaded bars, Toribio et. al.[28] argued that the solutions proposed by Levan and Royer were overly conservative, whereas solutions by Couroneau and Royer could be less conservative compared to the general trend when reviewing results proposed by several authors. The solutions proposed by Carpinteri was highlighted as a good option for stress mode I. For the present shaft we have to model crack sizes as small as 0.5mm, due to the presence of a surface defect. This corresponds to $\frac{a}{d} = 0.0014 - 0.0028$. Recent papers by Mikulski and Lassen[29], [30] suggests that LEFM can predict reasonable results from crack sizes as small as 0.1-0.5 mm even at weld notches. To accommodate analyses of such small cracks there is a need for additional datapoints to the set of geometry factors provided by Carpinteri. Based on this discussion a finite element analysis of a round bar was carried out in the present work. The objective was to provide additional datapoints to the dataset provided by Carpinteri, with subsequent curve fitting by least squares method for providing polynomial expressions as approximations for the geometry factors. The finite element analyses were performed in Abaqus where a quarter of a round bar with d=50mm was analyzed. The cracks were modelled at the symmetry plane of the round bar and two load cases, axial load and bending load were investigated separately for each combination of crack depth and crack shape. For the axial load case 1000N was applied to the free end of the bar, while for the bending load case 5000Nmm was applied to a reference point connected to the free end of the bar via a kinematic coupling. The J-integral was utilized for calculating the stress intensity factor at the deepest point A and close to the surface point C, where the built-in option in Abaqus of shifting the mid-side nodes near the crack front to quarter-point positions was utilized to simulate the stress singularity in the vicinity of the crack. The crack in the bar was meshed with a half circle of quadratic wedge elements around the crack front with further quadratic hexahedron elements in four layers outside as shown in Figure 10.

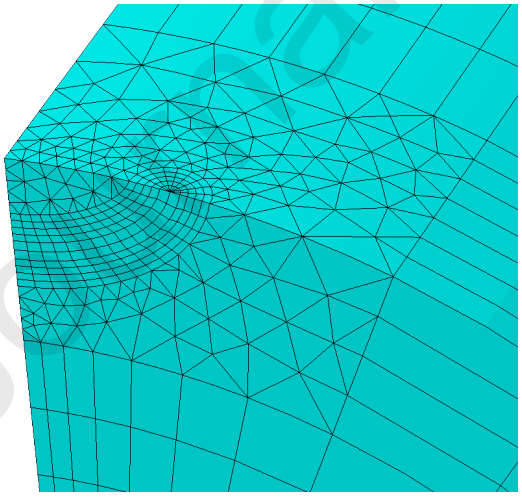

Figure 10 Mesh around crack with size and shape: a/d=0.5 a/c=0.6

20 analyses were performed where two values of a/d were investigated along with 5 different values of a/c for axial and bending load. The new datapoints are presented together with existing datapoints obtained by Carpinteri in Table 4 and Table 5, whereas the associated polynomial approximations are given in equations 12-15.

		Y(a/c,a/d) Axial stress						
		a/d						
		Present work		Carpinteri datapoints				
a/c		**0.02**	**0.05**	**0.1**	**0.2**	**0.3**	**0.4**	**0.5**
0.4	**A**	0.94	0.94	0.95	1.15	1.39	1.77	2.46
	C	0.63	0.59	0.72	0.91	1.17	1.58	2.31
0.5	**A**	0.88	0.88	0.91	1.1	1.32	1.66	2.3
	C	0.68	0.67	0.72	0.91	1.17	1.57	2.31
0.6	**A**	0.83	0.84	0.87	1.04	1.25	1.56	2.14
	C	0.72	0.72	0.72	0.91	1.17	1.56	2.26
0.8	**A**	0.74	0.74	0.79	0.93	1.07	1.3	1.75
	C	0.76	0.77	0.72	0.9	1.13	1.46	2.12
1	**A**	0.66	0.69	0.71	0.82	0.93	1.08	1.35
	C	0.76	0.76	0.71	0.86	1.03	1.3	1.84

Table 4 Geometry factors as function of crack depth and crack shape at location A and C for axial stress

		Y(a/c,a/d) Bending stress						
		a/d						
		Present work		Carpinteri datapoints				
a/c		**0.02**	**0.05**	**0.1**	**0.2**	**0.3**	**0.4**	**0.5**
0.4	**A**	0.92	0.88	0.78	0.8	0.82	0.91	1.08
	C	0.62	0.57	0.61	0.66	0.71	0.82	1.03
0.5	**A**	0.86	0.83	0.75	0.76	0.78	0.83	1.01
	C	0.68	0.65	0.64	0.68	0.74	0.83	1.05
0.6	**A**	0.81	0.78	0.71	0.72	0.73	0.78	0.92
	C	0.72	0.70	0.65	0.71	0.77	0.86	1.06
0.8	**A**	0.72	0.69	0.64	0.63	0.62	0.62	0.74
	C	0.75	0.75	0.64	0.72	0.77	0.86	1.07
1	**A**	0.64	0.64	0.58	0.55	0.5	0.5	0.52
	C	0.75	0.75	0.63	0.69	0.74	0.82	0.98

Table 5 Geometry factors as function of crack depth and crack shape at location A and C for bending stress

The fitted polynomials for axial loading are:

$$Y_{I,Fa}\left(\frac{a}{c},\frac{a}{d}\right) = 1.205 - 0.716\left(\frac{a}{c}\right) - 1.339\left(\frac{a}{d}\right) + 0.19\left(\frac{a}{c}\right)^2 + 0.73\left(\frac{a}{c}\right)\left(\frac{a}{d}\right) + 17.16\left(\frac{a}{d}\right)^2 - 0.13 - 0.2841\left(\frac{a}{c}\right)\left(\frac{a}{d}\right)^2 - 40.18\left(\frac{a}{d}\right)^3 - 2.136\left(\frac{a}{c}\right)^2\left(\frac{a}{d}\right)^2 - 6.817\left(\frac{a}{c}\right)\left(\frac{a}{d}\right)^3 + 51.78\left(\frac{a}{d}\right)^4 \quad (12)$$

$$Y_{I,Fc}\left(\frac{a}{c},\frac{a}{d}\right) = 0.211 + 1.336\left(\frac{a}{c}\right) + 2.204\left(\frac{a}{d}\right) - 0.728\left(\frac{a}{c}\right)^2 - 9.546\left(\frac{a}{c}\right)\left(\frac{a}{d}\right) + 11.84\left(\frac{a}{d}\right)^2 + 4.5\left(\frac{a}{d}\right) + 25.18\left(\frac{a}{c}\right)\left(\frac{a}{d}\right)^2 - 51.34\left(\frac{a}{d}\right)^3 - 12.1\left(\frac{a}{c}\right)^2\left(\frac{a}{d}\right)^2 - 12.45\left(\frac{a}{c}\right)\left(\frac{a}{d}\right)^3 + 66.75\left(\frac{a}{d}\right)^4 \quad (13)$$

And for the bending loading:

$$Y_{I,Ba}\left(\frac{a}{c},\frac{a}{d}\right) = 1.263 - 0.8196\left(\frac{a}{c}\right) - 4.088\left(\frac{a}{d}\right) + 0.2402\left(\frac{a}{c}\right)^2 + 3.383\left(\frac{a}{c}\right)\left(\frac{a}{d}\right) + 19.04\left(\frac{a}{d}\right)^2 - \left(\frac{a}{c}\right)^2\left(\frac{a}{d}\right) - 8.698\left(\frac{a}{c}\right)\left(\frac{a}{d}\right)^2 - 37.14\left(\frac{a}{d}\right)^3 + 0.06085\left(\frac{a}{c}\right)^2\left(\frac{a}{d}\right)^2 + 6.07\left(\frac{a}{c}\right)\left(\frac{a}{d}\right)^3 + 32.1 \quad (14)$$

$$Y_{I,Bc}\left(\frac{a}{c},\frac{a}{d}\right) = 0.2293 + 1.315\left(\frac{a}{c}\right) + 0.5773\left(\frac{a}{d}\right) - 0.7197\left(\frac{a}{c}\right)^2 - 6.075\left(\frac{a}{c}\right)\left(\frac{a}{d}\right) + 8.39\left(\frac{a}{d}\right)^2 + \left(\frac{a}{c}\right)^2\left(\frac{a}{d}\right) + 16.97\left(\frac{a}{c}\right)\left(\frac{a}{d}\right)^2 - 36.53\left(\frac{a}{d}\right)^3 - 4.423\left(\frac{a}{c}\right)^2\left(\frac{a}{d}\right)^2 - 12.52\left(\frac{a}{c}\right)\left(\frac{a}{d}\right)^3 + 43.38 \quad (15)$$

Figure 11 and Figure 12 shows comparisons between geometry functions calculated with the present proposed polynomials and results obtained by other authors at the deepest point of the crack A. The figures show that the proposed polynomial expressions give results close to the one proposed by Couroneau at small crack sizes when considering axial load, whereas for larger cracks the gap between Couroneau's results and the present polynomials increase. When considering bending loading the results from the polynomials are very similar to Couroneau. Geometry functions proposed by BS7910 has also been considered, where the values presented for different a/c relationships by BS7910 are lower than the results from the proposed polynomials and Couroneau's work for 0.8<a/c<1.0 for both axial and bending loading. The semi-circular option provided by BS7910 has also been included in the comparison which gives similar values to the polynomials at

a/c=1.0. However, only geometry functions for the deepest point are provided with this option which makes it unable to predict the crack shape development in addition to being less conservative for other crack aspect ratios than a/c=1.0.

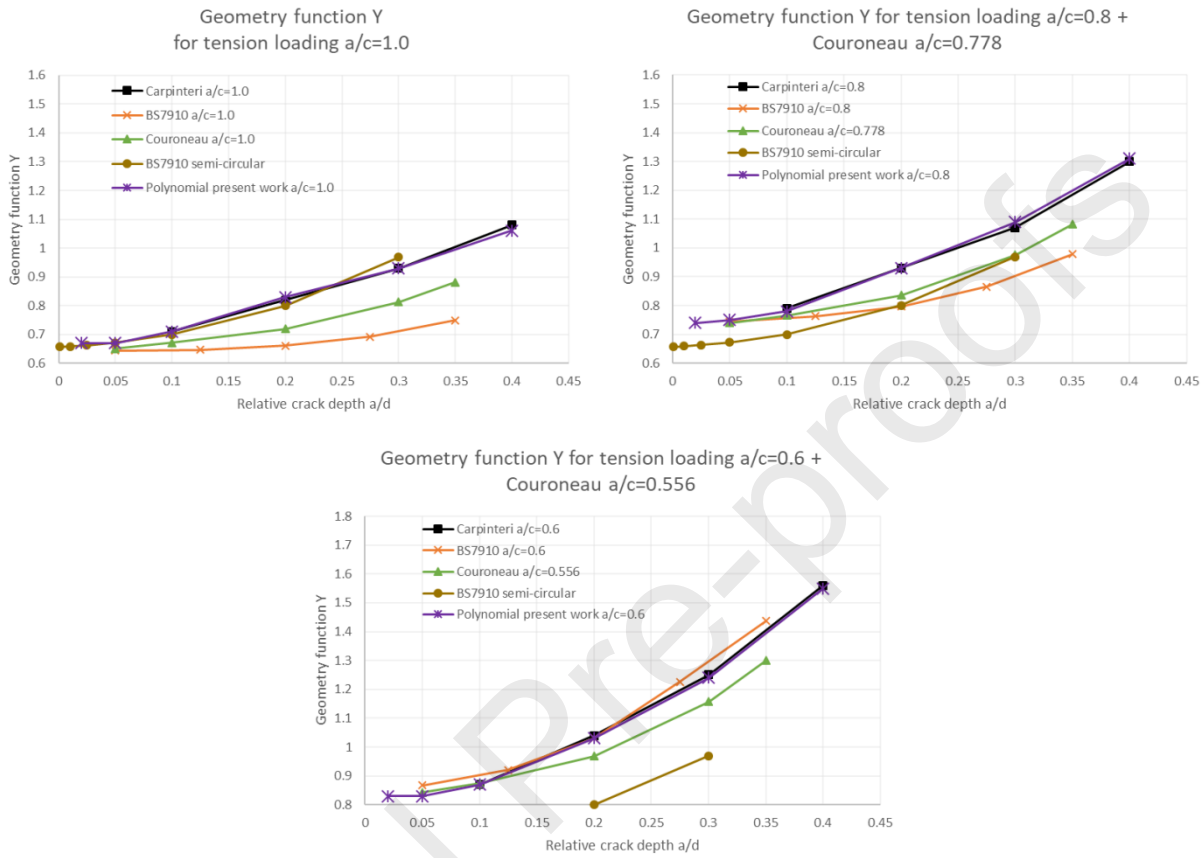

Figure 11 Geometry functions for tension loading at the deepest point A

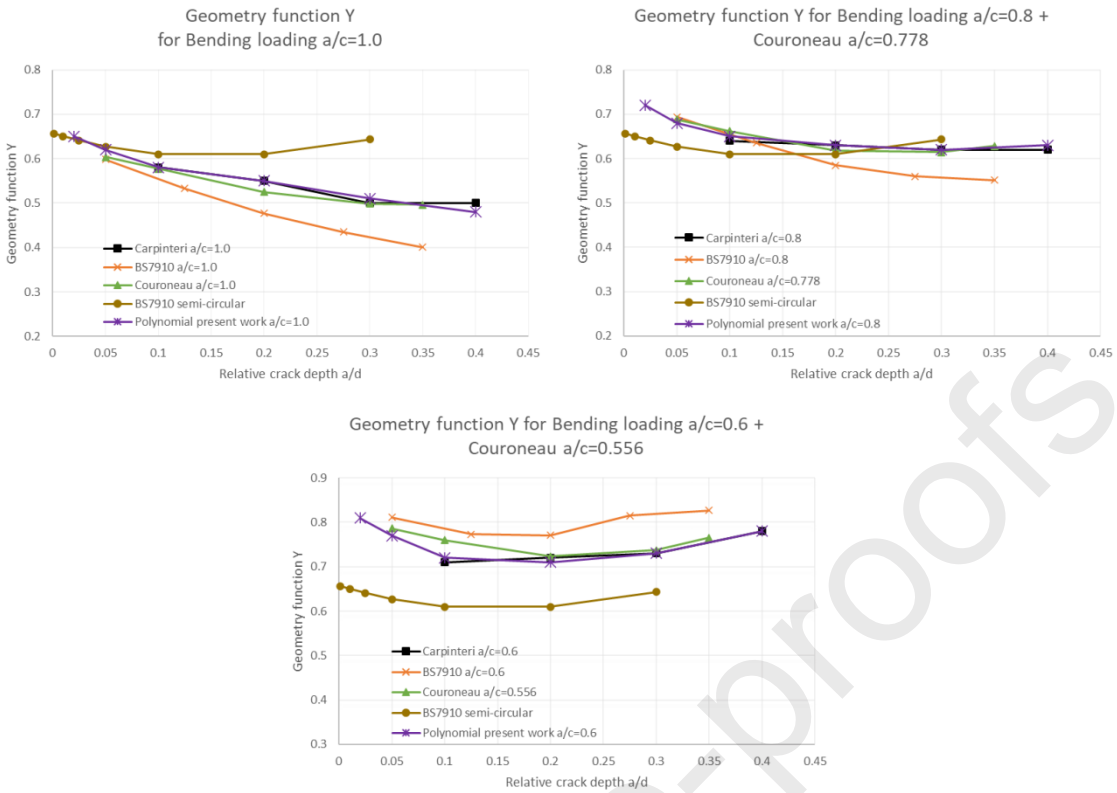

Figure 12 Geometry function for Bending loading at deepest point A

Based on the discussions above the proposed polynomials from the present work is considered an improved option to existing calculation models for the geometry factors. The polynomials provide values for smaller cracks which are still large enough such that LEFM can be applied. The results also compare well with established calculation models for larger cracks. Hence for the crack growth analyses for stress mode I in the present paper, these polynomials are utilized.

6.5 Calculations of geometry factors for stress mode II and III

Fewer investigations can be found in the literature regarding geometry factors for stress mode II and III. These geometry factors are important when initiating a discussion regarding mixed mode crack propagation. Investigations published by da Fonte and da Freitas[31] and Ismail et al[32] propose some values, but there are large gaps between the two works. Hence, similar analyses as described in section 6.4 are performed. Geometry factors for crack aspect ratios a/c= 0.8 and a/c= 0.6 are extracted, since this is close to the measured aspect ratios of the observed crack, and compared with the published work in [31], [32]. The comparison can be seen in Figure 13. At point A, the deepest point of the crack, the mode II stress intensity factor is 0 when the shaft is subject to torsional shear stress, whereas K_{III} has a non-zero value. At point C, close to the edge of the crack, both KII and KIII have non-zero values and will contribute to crack growth. The graphs show the discrepancies between the different sources. In the present work the geometry factors at point A will be utilized for crack growth analysis to investigate possible influence of K_{III} in the case of mixed stress mode crack propagation during the early growth of the crack (a/d<0.025). At this location the discrepancies are smaller than at point C. However, a variation between 0.6 – and 0.9 can be seen which underlines the uncertainty in this parameter. Hence, a pragmatic approach will be taken where several crack growth

analyses will be performed with different values of Y_{III}, where the parameter will be kept constant during each analysis.

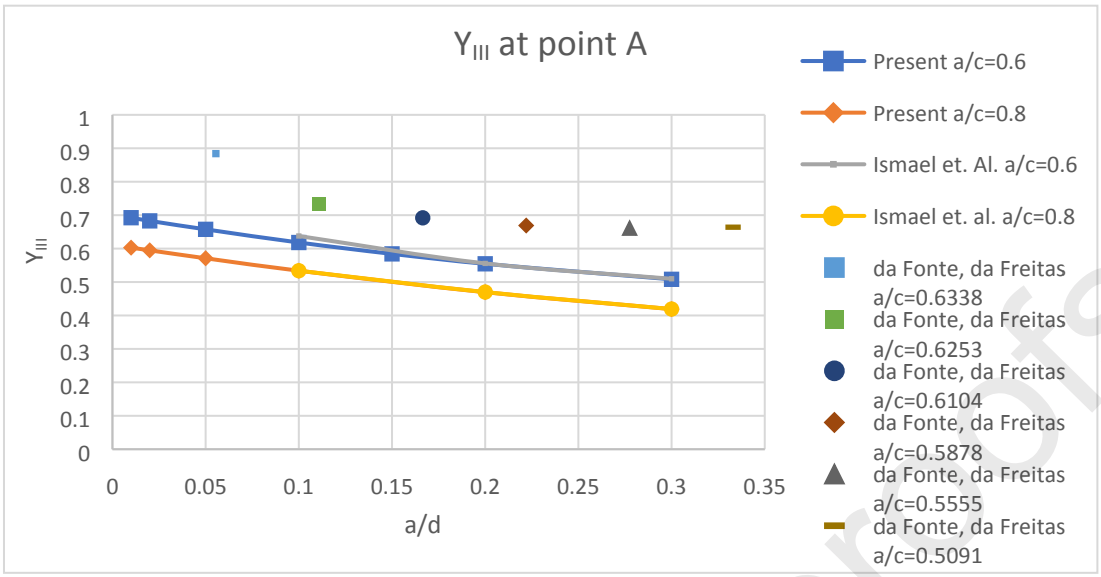

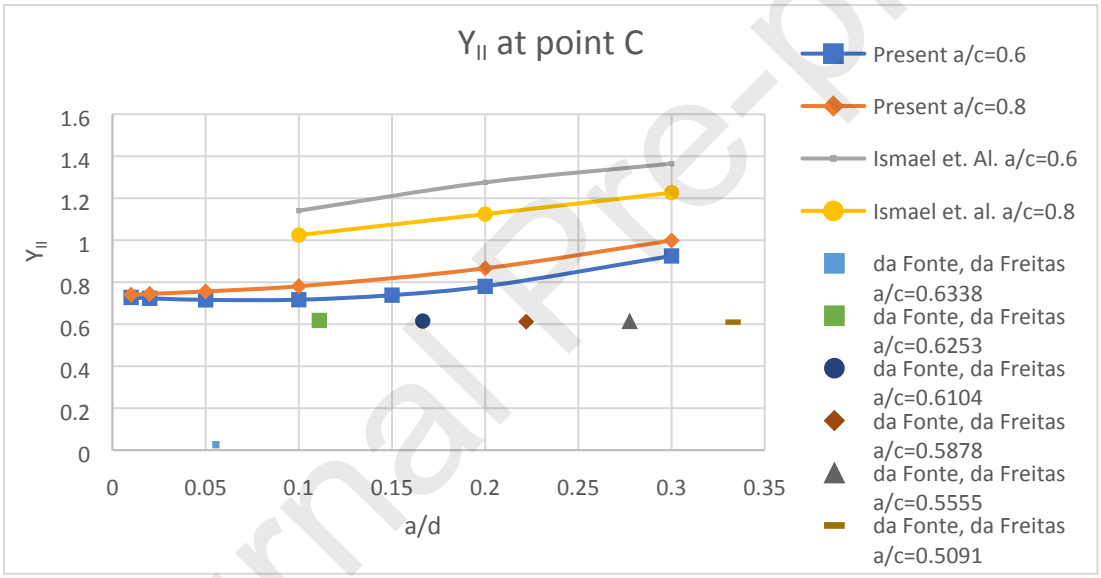

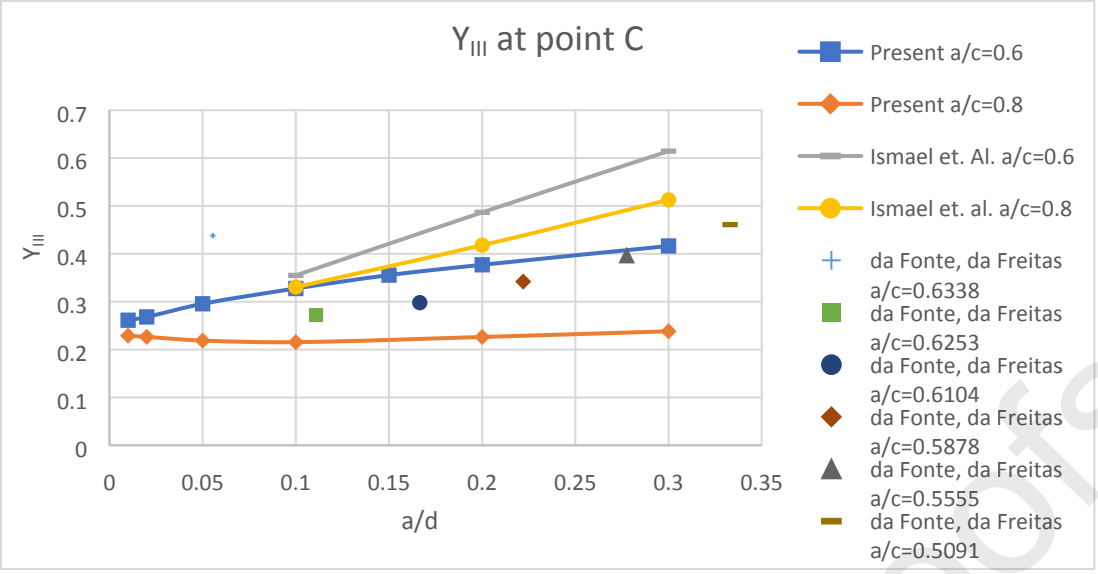

Figure 13 Mode II and III geometry factors

7 Simulation of the crack behavior

7.1 General considerations

The present crack behavior is characterized by the propagation of a single semi-elliptical shaped crack. The crack origin was determined at an initial surface defect which is modelled as a crack like flaw during the analyses described in the present section. The crack plane is most of the time 90 degrees to the shaft axis. At the end of the propagation there is a shift in the directions of the crack planes such that they approach 60 degrees with the shaft axis. In the present section we shall seek a fracture mechanics-based model that can simulate the detailed observations made in section 4.

Table 6 gives stress ranges and the corresponding number of cycles pr year utilized in the analyses. For the bending stresses, the number of cycles will be dependent on the source of the bending. As discussed, this could be bearing misalignment or lateral forces on the propeller. Since the source is not known it is assumed that a bending stress range occurs at each revolution of the shaft. The stress range is subsequently determined such that the model for crack growth analysis gives 20 months of fatigue life.

Table 6 Stress ranges utilized for fatigue crack growth calculations

	Torsion $\Delta\tau_T$ steady state	Bending $\Delta\sigma_B$
Stress Range [Mpa]	18	Ranges which predict 20 months fatigue life
Number of cycles 1 year	6.68E+07	6.68E+07

7.2 Stress intensity factors and crack growth parameters

The crack growth analyses have been performed with the following values of the material parameters [33]:

C = 1.83E-13 (for ΔK in $N/mm^{3/2}$) given as mean value

m = 3

The geometry factors for the SIF calculations are carried out by equations 12 to 15 for stress mode I.

The threshold value for the stress intensity factor ΔK_{th} given by DNVGL [33] and British Standard [15] is 63 $N/mm^{3/2}$ which is considered herein.

Final fracture is assumed when the crack depth has passed half the diameter of the shaft. At this crack depth the rate of propagation is so high that complete failure will occur within few cycles.

7.3 Simplified crack growth calculations for each loading mode separately

7.3.1 Preliminary assessment

Due to the fact that the stress spectra are not fully known it is chosen to do some simplified preliminary crack growth analysis to point out which of the stress spectra that has been the dominant one. The likely influence of each separate loading mode is based on comparison between crack behavior according to the models and the observations made during the failure investigation. Emphasis is on the crack shape and the inclination of the crack planes.

7.3.2 Pure torsional loading mode

For this foreseen loading mode, it is expected that the crack plane will follow a 45 degrees plane as discussed earlier. The observation is that the crack planes had an angle close to 90 degrees up to a crack depth of 9 mm. This first growth phase is in fact about 50-75% of the total fatigue life. From these figures it can be concluded already from the start that the torsional loading mode cannot have been the dominant one. With the given shear stress ranges close to 18 MPa the principal stress variations at the 45 degrees plane are also close to 18 MPa.

The highest value of ΔK_I is then 36 $N/mm^{3/2}$ when assuming an initial crack depth of 1 mm and an aspect ratio a/c as low as 0.167. This is far below ΔK_{th} which indicates that no crack growth will occur. Even if the stress cycles at these low values of ΔK were assumed fully damaging the crack would only have grown to a depth of 2.5mm i.e. an advancement of 1.5mm after 20 months in service.

On the other hand, the shear stress ranges from the barred speed range reaches a magnitude of close to 160MPa. If considering only the stresses from this barred speed range and assuming 120000 cycles per year ($3*10^6$cycles/25 years), using initial crack depth of 1mm and aspect ratio of 0.167 the crack reaches 5.55mm after 20 months in service. At this point the stress intensity factor range following the steady state shear stresses is still below the threshold value. This indicates that the stresses from the barred speed range may have been an important contributor to the crack growth but also that other contributions would be needed to achieve the rapid growth observed on the shaft.

7.3.3 Pure bending Loading mode

For this loading mode it is expected that the crack planes have a normal vector that coincides with the shaft length axis. This is in agreement with the present observations. The stress ranges are unknown, but it is determined such that the simulated fatigue life is close to 20 months. This is done by introducing an equivalent constant amplitude stress range which simulates the same fatigue damage as the actual stress ranges in the spectrum. This gives an equivalent stress range within the interval 31.5 MPa to 42 MPa dependent on the initial crack size and crack shape. Several analyses have been performed where two initial crack depths have been used; 0.5 mm and 1 mm, and three initial crack aspect ratios have been used; 1, 0.25 and 0.167. These crack sizes are chosen to simulate the irregular surface defect that was found by microscopy examination. The values for the aspect ratios are randomly selected to investigate possible crack shape developments. All the analyses performed give initial ΔK_I values close to or below the threshold level. The actual number of cycles experienced during the 20 months of service is unknown. Hence, this could be an indication of higher stress levels and a smaller number of cycles experienced. However, since the analyses are based on an equivalent stress range, the initial ΔK_I value that is slightly below the threshold level has been considered to contribute to the crack growth.

A typical growth history obtained by the simulations is shown in Figure 14. An important finding is that the semi-elliptical shapes of the crack front at various stages during the growth are in good agreement with the observed shapes on the fractured surface. In Figure 15, the observed aspect ratios are displayed with x and the simulated development of the aspect ratios is given by the curves. A simulation performed with axial stress is also included for reference which shows a much poorer agreement with the measured points. Figure 16 shows sketches of the crack shape development from different initial aspect ratios. All these findings are supporting the assumption that the crack growth is mainly driven by normal stress variations imposed by alternating bending stresses.

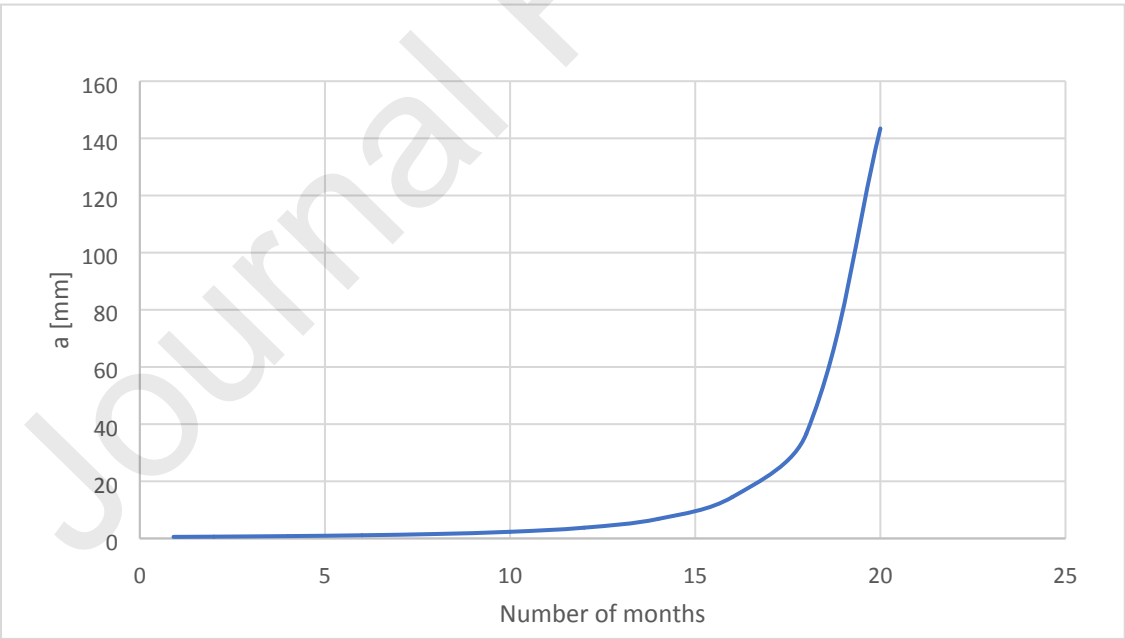

Figure 14 Typical crack growth curve for the simulated crack growth

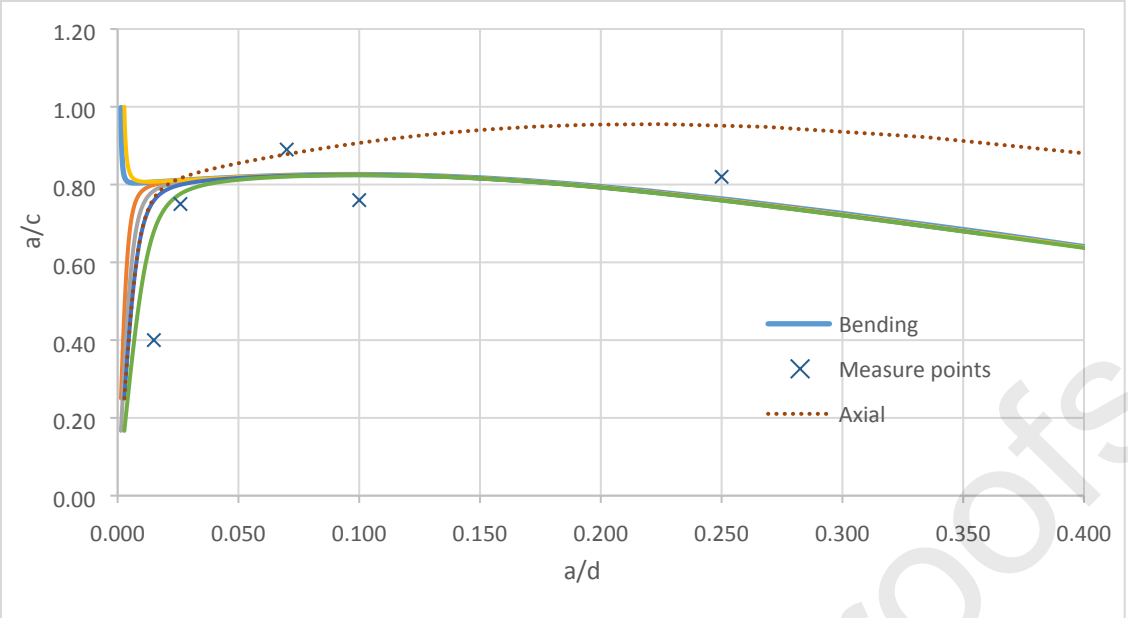

Figure 15 Simulated crack shape development for bending stress compared to measured crack shapes

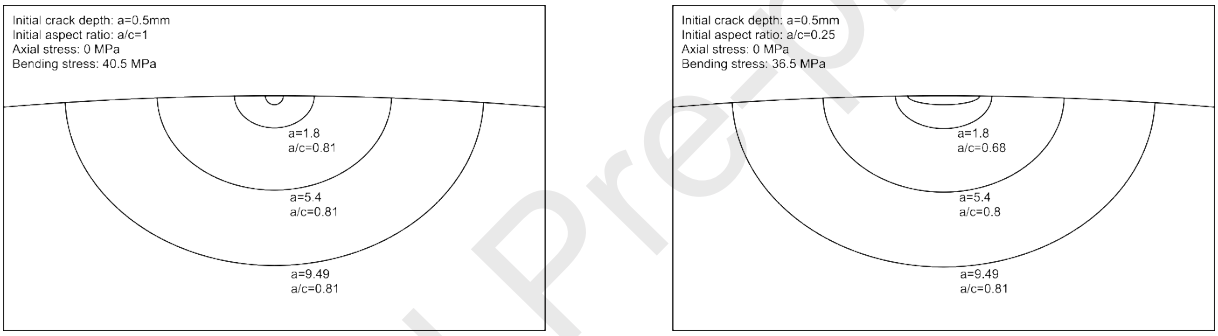

Figure 16 Simulated crack shape development from different initial aspect ratios

7.4 Investigation of crack growth due to a multiaxial stress state

7.4.1 Defining the problem and clarifying the assumptions

The fatigue failure is caused by crack propagation primarily under stress mode I. By investigating the possible loading modes separately, it can be concluded that the dominant loading mode is unintentional bending in the shaft. From an engineering point of view, one may consider the analyses to be sufficient for practical conclusion. However, two research questions emerge that merit a final discussion:

- During the major time of the crack growth, i.e. from an initial crack to a crack depth of 9 mm do the shear stresses accelerate the crack growth?
- Why is there a shift in the crack plane angle in the last part of the crack growth when the crack depth passes 9 mm?

The first phase above is about 50-75% of the propagation life and will be modelled with Paris Law given by equation 5, utilizing the equivalent stress intensity factor for mixed mode loading given by equation 9. For the last phase, the crack plane angle changes from 90 to 60 degrees with respect to the shaft axis. The remaining fatigue propagation life at this stage is approximately 25-50%. It can be argued that modelling this last fraction of the crack propagation life has little practical value.

However, from a theoretical point of view the change in the crack plane orientation is interesting. We will pursue this last phase based on the consideration given in point 3 in the beginning of section 6.2.

7.4.2 Combined stress spectrum with in-phase shear and bending stresses (3a)

In the present section the influence of shear stresses on the crack growth rate is analyzed for a crack depth up to 9 mm. The crack plane is assumed to remain 90 degrees to the shaft axis as stress mode I is assumed to be the dominant loading mode. The shear stress range of approximately 18 MPa found from measurements of steady state vibrational torsional stress are combined in-phase with the normal stress ranges due to bending. The two contributions are combined in an equivalent stress intensity factor for mixed mode crack growth given by Equation 9. This scenario was denoted 3a in section 6.2. As this represents the steady state condition of the shaft rotation, it is assumed that the number of cycles can be obtained from the RPM at normal speed. Analyses were performed with an initial crack depth of 1mm and an initial aspect ratio a/c of 0.167. A bending stress range of 31MPa were included in the first analyses for comparison with the pure bending case which leads to fracture after 20 months in service. Different values of the geometry factor Y_{III} were attempted due to the high uncertainty in this parameter. The results are shown in Figure 17. As can be seen the torsional shear stress ranges may have played an important role, the bending stress variation may have been less than assumed due to the imposed shear stress contribution to crack growth acceleration.

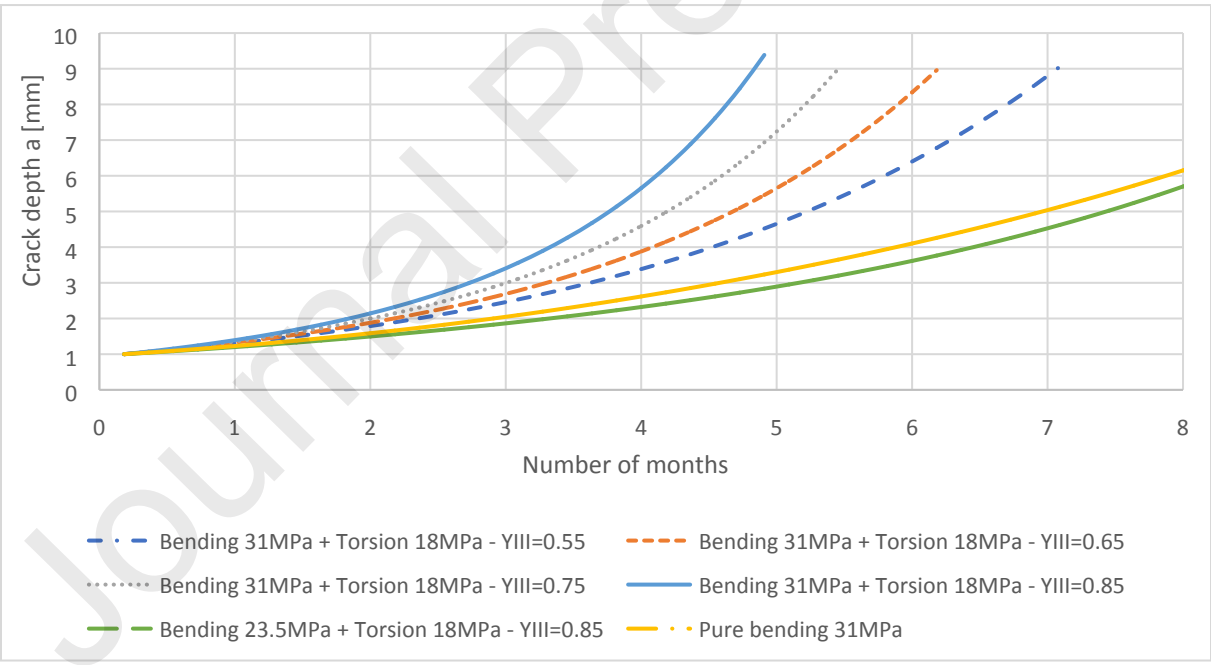

Figure 17 Mixed mode crack growth analyses utilizing ΔK_{eq} compared with pure bending case

7.4.3 Combined stress spectrum with in-phase shear and bending stresses (3b)

In the present case we shall assume similar stress situation as in section 7.4.2 but the assumption for the crack plane orientation is changed. Now it is assumed that the largest principal stress variation

will govern the crack plane orientation. This scenario was denoted 3b in section 6.2. In the following analysis we shall seek the crack growth from an initial crack depth to failure. Special focus is on the last phase from a depth of 9 mm to final fracture. The stress ranges are selected such that the principal stress direction calculated from the stress components has an angle of 30 degrees relative to the shaft axis. Hence, the predicted crack plane angle will be 60 degrees relative to the shaft axis which agrees with the observed crack plane. In addition, the selected stress ranges should give the predicted fatigue life of approximately 20 months. The following stress ranges fulfill these requirements: $\Delta\sigma_B$=21MPa and $\Delta\tau_T$=18MPa, where the initial crack depth is 1mm and with an initial aspect ratio a/c of 0.167. Figure 18 shows a comparison between the mixed stress mode model and the principal stress model. As can be seen there are very small differences between the crack growth curves. Hence, a shift from model 3a to model 3b at a crack depth of 9mm will predict almost the same fatigue life as each of the models separately. Further, the stress intensity factor ranges for the two different models are displayed in Figure 19. It should be noted that the equivalent stress intensity factor is based on YIII=0.85 which is highly uncertain. As previous analyses and the literature study has shown this parameter might be lower than the value utilized in this section.

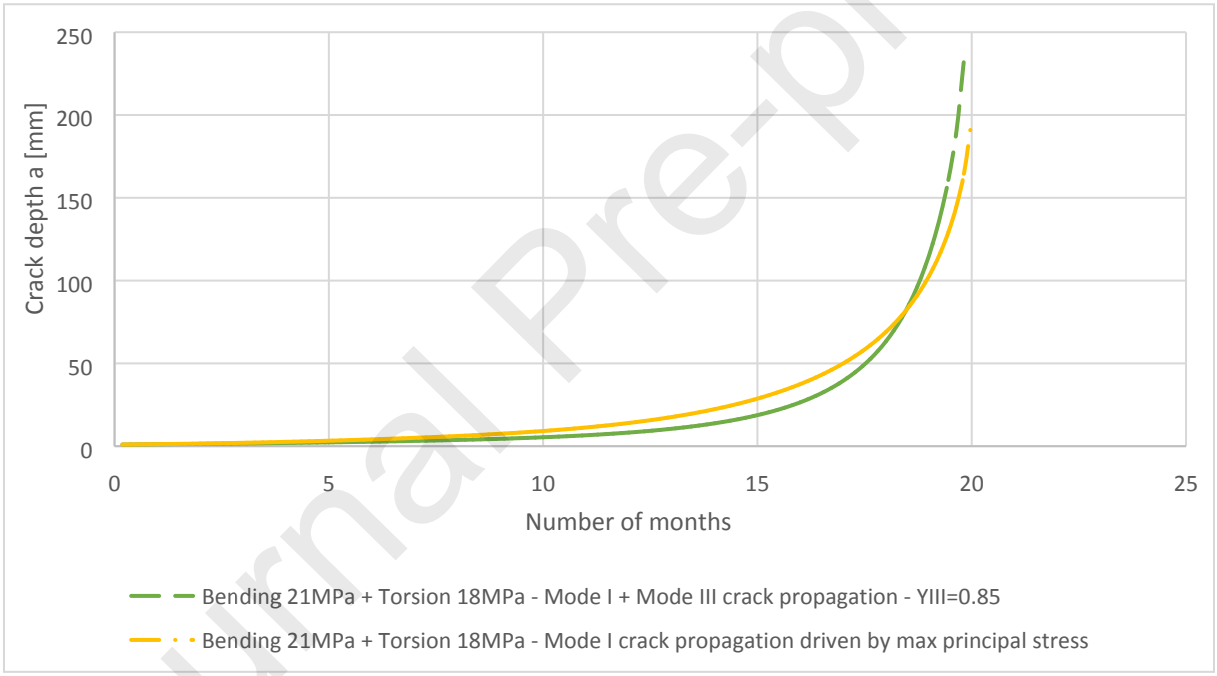

Figure 18 Crack growth predictions with scenario 3a and 3b

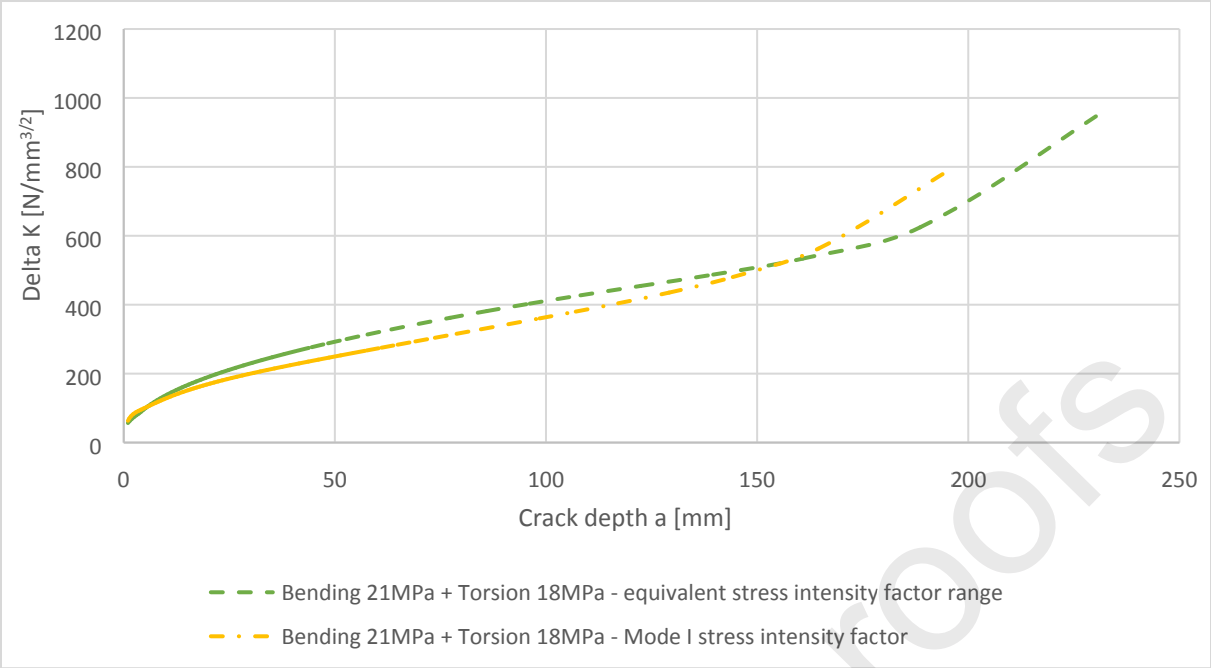

Figure 19 Stress intensity factor range for scenario 3a and 3b

8 Final discussion and conclusion

The fracture of the intermediate propeller shaft is clearly recognized as a fatigue failure. The facture occurred in the uniform part of the shaft and not in vicinity of any notch stress concentration. From observations on the fractured surfaces it is concluded that fatigue crack growth is the main damage mechanism. Due to the presence of a surface defect the long crack initiation phase usually present for such forged components in high strength steel seems to be lost. The short fatigue life consists mainly of a crack growth phase.

The bending loading mode is identified as the dominant driving mechanism for most of the crack growth. This conclusion is drawn based on the crack plane orientation and the crack shape development characterized by the aspect ratio a/c. The variations of shear stresses may have accelerated the crack growth.

In the analysis it is demonstrated that the recent advances in LEFM methodology makes it possible to reconstruct and simulate the crack propagation in the shaft under stress mode I. However, SIF calculations had to be supplied for the small semi-elliptical surface cracks for the early crack growth. The observed crack shape development was modelled successfully whereas the ultimate change in the crack plane angle cannot be predicted by a uniaxial stress model.

An attempt was made to establish a multi-axial stress crack growth model that could predict the observed change in crack plane angle that occurred at a crack depth of 9 mm. The model gave a likely explanation for the change of crack plane orientation. However, the exact timing for the change of angle cannot be determined. There is at present no theoretical multi-axial model with enough experimental evidence that can predict at which stage shift in the crack plane will take place.

It is concluded that an initial flaw of 0.5 to 1 mm was present at the shaft surface. This was corroborated by microscopy. The combination of unintentional bending stress and the existence of a flaw led to a significant reduction in fatigue life compared to fatigue predictions following the S-N method. The origin of the initial flaw is unknown, but it highlights the importance of quality assurance procedures at the fabrication yards and during maintenance work to ensure that surface flaws on shafts are avoided. The presence of the initial flaw is the root cause of the fatigue failure.

Stress measurements which could reveal fluctuating bending stresses are also recommended as a risk reduction measure. Severe fluctuating bending stresses can be introduced by propeller lateral forces and bending of the hull beam. These stress variations are difficult to predict during design stage of the shaft.

9 References

[1] B. J. Vartdal, T. Gjestland, and T. I. Arvidsen, “Lateral Propeller Forces and their Effects on Shaft Bearings,” in *First International Symposium on Marine Propulsors*, 2009.

[2] DNVGL, “DNVGL Rules for classification of ships Pt.4 Ch.4 Rotating machinery - power transmission,” 2017.

[3] DNVGL, “DNVGL-CG-0038 Calculation of shafts in marine applications,” 2015.

[4] L. Murawski, “Shaft line alignment analysis taking ship construction flexibility and deformations into consideration,” *Mar. Struct.*, vol. 18, no. 1, pp. 62–84, 2005.

[5] Y. Batrak, “Lateral Vibration Prediction Issues,” 2011.

[6] D. Socie, “Multiaxial Fatigue Damage Models,” *J. Eng. Mater. Technol.*, vol. 109, no. 4, pp. 293–298, Oct. 1987.

[7] Z.-R. Wu, X.-T. Hu, and Y.-D. Song, “Multiaxial fatigue life prediction for titanium alloy TC4 under proportional and nonproportional loading,” *Int. J. Fatigue*, vol. 59, pp. 170–175, 2014.

[8] C. Baptista, A. Reis, and A. Nussbaumer, “Probabilistic S-N curves for constant and variable amplitude,” *Int. J. Fatigue*, vol. 101, pp. 312–327, 2017.

[9] P. Chowdhury and H. Sehitoglu, “Mechanisms of fatigue crack growth – a critical digest of theoretical developments,” *Fatigue Fract. Eng. Mater. Struct.*, vol. 39, no. 6, pp. 652–674, Jun. 2016.

[10] K. J. Miller, “The Three Thresholds for Fatigue Crack Propagation,” in *Fatigue and Fracture Mechanics: 27th Volume*, R. S. Piascik, J. C. Newman, and N. E. Dowling, Eds. West Conshohocken, PA: ASTM International, 1997, pp. 267–286.

[11] K. J. MILLER, “THE SHORT CRACK PROBLEM,” *Fatigue Fract. Eng. Mater. Struct.*, vol. 5, no. 3, pp. 223–232, Jul. 1982.

[12] A. Carpinteri, “ELLIPTICAL-ARC SURFACE CRACKS IN ROUND BARS,” *Fatigue Fract. Eng. Mater. Struct.*, vol. 15, no. 11, pp. 1141–1153, Nov. 1992.

[13] A. Levan and J. Royer, “Part-circular surface cracks in round bars under tension, bending and twisting,” *Int. J. Fract.*, vol. 61, no. 1, pp. 71–99, 1993.

[14] N. Couroneau and J. Royer, “Simplified model for the fatigue growth analysis of surface cracks in round bars under mode I,” *Int. J. Fatigue*, vol. 20, no. 10, pp. 711–718, 1998.

[15] British Standards Institution, “BS 7910:2013+A1:2015, Guide to methods for assessing the acceptability of flaws in metallic structures,” 2015.

[16] A. Carpinteri, “Shape change of surface cracks in round bars under cyclic axial loading,” *Int. J. Fatigue*, vol. 15, no. 1, pp. 21–26, 1993.

[17] M. W. BROWN and K. J. MILLER, “INITIATION AND GROWTH OF CRACKS IN BIAXIAL FATIGUE,” *Fatigue Fract. Eng. Mater. Struct.*, vol. 1, no. 2, pp. 231–246, Mar. 1979.

[18] L. P. Pook, “The fatigue crack direction and threshold behaviour of mild steel under mixed mode I and III loading,” *Int. J. Fatigue*, vol. 7, no. 1, pp. 21–30, 1985.

[19] D. Broek, *The practical use of fracture mechanics.* 1989.

[20] J. R. Yates, M. Zanganeh, R. A. Tomlinson, M. W. Brown, and F. A. D. Garrido, “Crack paths under mixed mode loading,” *Eng. Fract. Mech.*, vol. 75, no. 3–4, pp. 319–330, Feb. 2008.

[21] J. Qian and A. Fatemi, “Mixed mode fatigue crack growth: A literature survey,” *Eng. Fract. Mech.*, vol. 55, no. 6, pp. 969–990, 1996.

[22] G. C. Sih, *Mechanics of fracture initiation and propagation: surface and volume energy density applied as failure criterion*. Kluwer Academic, 1991.

[23] H. A. Richard, M. Fulland, F. G. Buchholz, and M. Schöllmann, “3D Fracture Criteria for Structures with Cracks,” *steel Res. Int.*, vol. 74, no. 8, pp. 491–497, Aug. 2003.

[24] H. A. RICHARD, M. FULLAND, and M. SANDER, “Theoretical crack path prediction,” *Fatigue Fract. Eng. Mater. Struct.*, vol. 28, no. 1-2, pp. 3–12, Jan. 2005.

[25] C. F. Arisoy, G. Başman, and M. K. Şeşen, “Failure of a 17-4 PH stainless steel sailboat propeller shaft,” *Eng. Fail. Anal.*, vol. 10, no. 6, pp. 711–717, 2003.

[26] P. Paris and F. Erdogan, “A Critical Analysis of Crack Propagation Laws,” *J. Basic Eng.*, vol. 85, no. 4, pp. 528–533, Dec. 1963.

[27] Y.-S. Shih and J.-J. Chen, “Analysis of fatigue crack growth on a cracked shaft,” *Int. J. Fatigue*, vol. 19, pp. 477–485, 1997.

[28] J. Toribio, N. Álvarez, B. González, and J. C. Matos, “A critical review of stress intensity factor solutions for surface cracks in round bars subjected to tension loading,” *Eng. Fail. Anal.*, vol. 16, no. 3, pp. 794–809, 2009.

[29] Z. Mikulski and T. Lassen, “Fatigue crack initiation and subsequent crack growth in fillet welded steel joints,” *Int. J. Fatigue*, vol. 120, pp. 303–318, 2019.

[30] Z. Mikulski and T. Lassen, “Crack growth in fillet welded steel joints subjected to membrane and bending loading modes,” *Eng. Fract. Mech.*, vol. 235, p. 107190, 2020.

[31] M. Da Fonte and M. De Freitas, “Stress intensity factors for semi-elliptical surface cracks in round bars under bending and torsion,” *Int. J. Fatigue*, vol. 21, no. 5, pp. 457–463, 1999.

[32] A. E. Ismail, A. K. Ariffin, S. Abdullah, and M. J. Ghazali, “Stress intensity factors for surface cracks in round bar under single and combined loadings,” *Meccanica*, vol. 47, no. 5, pp. 1141–1156, 2012.

[33] DNVGL, “DNVGL-RP-C210 Probabilistic methods for planning of inspection for fatigue cracks in offshore structures,” 2015.

Highlights

- Enhanced expressions for calculating stress intensity factors for round bars proposed
- Crack growth simulations compared with observed crack development
- Multi-axial crack tip stress states included in analyses and discussed

Declaration of interests

☒ The authors declare that they have no known competing financial interests or personal relationships that could have appeared to influence the work reported in this paper.

☐The authors declare the following financial interests/personal relationships which may be considered as potential competing interests: